Lidar-observed enhancement of aerosols in UTLS over the Tibetan Plateau induced by the Nabro volcano eruption

Q. S. He[1], C. C. Li[2], J. Z. Ma[3], H. Q. Wang[4], X. L. Yan[3], J. Lu[5], Z. R. Liang[1], and G. M. Qi[6]

[1]Shanghai Meteorological Service, Shanghai, China

[2]Department of Atmospheric and Oceanic Sciences, School of Physics, Peking University, Beijing, China

[3]Chinese Academy of Meteorological Sciences, Beijing, China

[4]College of Environmental Science and Engineering, Donghua University, Shanghai, China

[5]School of Computer and Software, Nanjing University of Information Science and Technology, Nanjing, China

[6]Germu Meteorological Bureau, Qinghai, China

Correspondence to: C. C. Li (ccli@pku.edu.cn)

Abstract.

Vertical profiles of aerosol extinction coefficients were measured by an Micro Pulse Lidar at Naqu (31.5 °N, 92.1 °E, 4508m a.m.s.l.), a meteorological station located on the central part of the Tibetan Plateau during summer 2011. Observations show a persistent maximum in aerosol extinction coefficients in the upper troposphere–lower stratosphere (UTLS). These aerosol layers were generally located at an altitude of 18–19 km a.m.s.l., 1–2 km higher than the tropopause, with broad layer depth ranging approximately 3–4 km and scattering ratio of 4-9. Daily averaged aerosol optical depths (AODs) of the enhanced aerosol layers in UTLS over the Tibetan Plateau varied from 0.007 to 0.030, in agreement with globally averaged levels of 0.018 ± 0.009 at 532 nm from previous observations, but the percentage contributions of the enhanced aerosol layers to the total AOD over the Tibetan Plateau are higher than those observed elsewhere. The aerosol layers in UTLS wore off gradually with the reducing intensity of the Asian monsoon over the Tibetan Plateau at the end of August. The eruption of Nabro volcano on 13 June 2011 is considered as an important factor to explain the enhancement of tropopause aerosols observed this summer over the Tibetan Plateau.

1 Introduction

Aerosols in the upper troposphere–lower stratosphere (UTLS) play an important role in the global/regional climate system and the geochemical cycle (Hanson et al., 1994; Borrmann et al., 1997; Solomon et al., 1997). They also influence atmospheric ozone budgets through providing surface areas for efficient heterogeneous reactions (Keim et al., 1996; Solomon, 1999).

Volcanic eruption, though as occasional event, can inject amounts of ash and sulfur dioxide (SO_2) into the stratosphere, and the injected SO_2 are oxidized to sulfuric acid particles through homogeneous nucleation (Wu et al., 1994). The Nabro stratovolcano in Eritrea, northeastern Africa, erupted on 13 June 2011, injecting approximately 1.3 teragrams of SO_2 to altitudes of 9 to 14 kilometers in the upper troposphere, which resulted in a large aerosol enhancement in the stratosphere (Bourassa et al., 2012). This event has been observed by lidar networks such as EARLINET, MPLNET and the Network for the Detection of Atmospheric Composition Change (NDACC) with independent lidar groups and satellite Cloud–Aerosol Lidar and Infrared Pathfinder Satellite Observations (CALIPSO) to track the evolution of the stratospheric aerosol layer in various parts of the globe (Uchino et al., 2012; Sawamura et al., 2013), and other instruments, such as the Infrared Atmospheric Sounding Interferometer (Clarisse et al., 2013) and the ground-based spectrometry of twilight sky brightness (Tukiainen et al., 2013). Bourassa et al. (2012) found that the aerosol enhancement built while remaining confined for several weeks to the region between central Asia and the Middle East after eruption of Nabro volcano using the limb scanning Optical Spectrograph and Infra-Red Imaging System (OSIRIS) satellite instrument.

It is also should be noted that aerosol enhancements in UTLS over the Tibetan Plateau have already been observed by many researchers before eruption of Nabro volcano. Using the Stratospheric Aerosol and Gas Experiment II (SAGE II) data, Li et al. (2001) found that aerosol concentrations near 100 hPa are higher over the Tibetan Plateau than over China's central and northern regions in summer. Recent observations by balloon-borne optical particle counter (Tobo et al.,2007) and aircraft-borne measurements (Keim et al., 1996; Solomon, 1997) showed that soot-containing liquid aerosols with the major components of fine particles may also affect the aerosol layer near the tropopause. Appearance of cold tropopause in the upper troposphere (possibly in the lower stratosphere also) has been considered as an important factor to explain the enhancement of tropopause aerosols observed in summer over the Plateau (Kim et al., 2003). This observational fact is important from the point view of heterogeneous reactions on aerosol surfaces since gas-to-particle conversion processes are generally more active in low temperature. During summer, the elevated surface heating and rising air associated with persistent deep convection over the Tibetan Plateau leads to anticyclonic circulation and divergence in the UTLS (Yanai et al., 1992; Hoskins and Rodwell, 1995; Highwood and Hoskins, 1998), where persistently enhanced pollutants such as aerosols, CO, methane and nitrogen oxides, as well as water vapor, can be linked to the rapid vertical transport of surface air from Asia, India and Indonesia in deep convection and confinement by strong anticyclonic circulation (Rosenlof et al., 1997; Jackson et al., 1998; Dethof et al., 1999; Park et al., 2004; Filipiak et al., 2005; Li et al., 2005a; Fu et al., 2006).

The aerosols from Nabro eruption might overlap with the background tropopause aerosols by deep convection in summer as mentioned previous studies, changing their properties and evolvement in UTLS over the Plateau. A clarification of the states that aerosols transport into and disperse out of the UTLS over the Plateau is an important step toward understanding volcanic emission influences on hydration and chemical composition in the global stratosphere. Knowing the height dependence of the aerosol changes is important for understanding the volcano responsible for the transport of aerosols from the troposphere to the stratosphere over the Tibetan Plateau; however, a variety of aerosol vertical distributions and optical properties over the Tibetan Plateau has not been assessed in a satisfactory manner due to lack of continuous direct observations.

The vertical distributions of aerosol extinction coefficients were measured over the Tibetan Plateau in the summer of 2011, as part of the project “Tibetan Ozone, Aerosol and Radiation” (TOAR). In this study, the lidar and radiosonde measurement results are presented and compared with satellite data. We find a persistent maximum in aerosol extinction coefficients in the UTLS within the anticyclone, and show that such aerosol accumulation can be linked to the eruption of Nabro volcano. These results indicate that volcanic aerosol dispersed with the weakening of Tibetan anticyclonic circulation could primarily affect aerosol and hence radiation properties near the tropopause over the Tibetan Plateau.

2 Measurements and Data

2.1 Micro Pulse Lidar

An eye safe, compact, solid-state Micro Pulse Lidar (MPL-4B, Sigma Space Corp., USA) was operated at the Naqu Meteorological Bureau (31.5°N, 92.1°E, 4508m a.m.s.l.) on the central part of the Tibetan Plateau. The MPL is a backscatter lidar which uses an Nd:YLF laser with an output power of 12 μJ at 532nm and 2500 Hz repetition rate. The diameter of the receiving telescope is 20 cm, and the field of view is 0.1 mrad. The vertical resolution of the lidar observation is 30m, and the integration time is 30 s. Data obtained on the cloud-free days during nighttime were selected in order to avoid the disturbance of cloud and/or rain to column-averaged lidar ratio and solar noise.

In general, the inversion of the LIDAR profile is based on the solution of the single scattering LIDAR equation:

$$P(r) = O_c(r)CE\frac{\beta(r)}{r^2}\exp[-2\int_0^r \sigma(z)dz] \quad (1)$$

where r is the range, C is the LIDAR constant, which incorporates the transmission and the detection efficiency, and E is the laser pulse energy. $\beta(r)$ represents the total backscattering coefficient $\beta(r)= \beta_m(r)+ \beta_a(r)$, $\sigma(r)$ is the total extinction coefficient $\sigma(r)= \sigma_m(r)+ \sigma_a(r)$, $\beta_a(r)$ and $\sigma_a(r)$ are aerosol backscattering and extinction coefficients, respectively. $\beta_m(r)$ and $\sigma_m(r)$ are molecular contributions to the backscattering and the extinction coefficients, respectively. They can be evaluated by the Rayleigh-scattering theory from the Standard Atmosphere 1976 (NASA, 1976).

But here the molecular extinction coefficients are evaluated using temperature and pressure from the radiosondes released at the lidar field site twice a day. $O_c(r)$ is the overlap correction as a function of the range caused by field-of-view conflicts in the transceiver system. Systematic errors of P(r) were mainly observed in the lowest altitudes where an incomplete overlap between the emitted laser beam and the telescope field-of-view can led to an underestimation of aerosol backscatter and extinction coefficients. Since the majority of aerosols are contained in the first several kilometers of the atmosphere, the overlap problem must be solved. Overlap is typically solved experimentally, using techniques outlined by Campbell et al. (2002). The starting point is an averaged data sample where the system is pointed horizontally with no obscuration. By choosing a time when the atmosphere is well mixed, such as late afternoon, when the aerosol loading is low, backscattering through the layer is roughly assumed to be constant with range (i.e., the target layer is assumed to be homogeneous). The similar overlap calibration was carried out at the beginning of this field experiment.

The vertical profile of aerosol extinction coefficient σ_a is determined by a near end approach in solving the lidar equation as proposed by Fernald(1984). Considered the period of TOAR campaign was only two months after eruption of Nabro volcano, volcanic aerosols were still freshly nucleated particles with small size. The lidar ratios should therefore feature rather high (Müller et al., 2007). Sawamura et al. (2013) employed the mean lidar ratio value of 50 sr at 532 nm for most groups of global lidar networks to trace the evolution of the stratospheric aerosol layer from Nabro volcano eruption. Therefore, a column averaged lidar ratio of 50 sr is assumed for all measurements in this study.

We identify the boundaries of aerosol layer in the UTLS from the lidar extinction coefficient profiles. The lowest bin with σ_a=0.002 km^{-1} above 18 km is identified as the top of aerosol layer H_t and the bin with minimum value of σ_a between 10 km and 16 km as the layer base H_b. The visible optical depth of the aerosol layer is derived by integrating the values of σ_a between H_b and H_t.

2.2 Radiosonde Observations

During the field campaigns, 76 L-band (GTS1) electronic radiosondes (Nanjing Bridge Machinery Co., Ltd., China) were launched to provide vertical profiles of pressure, temperature, and humidity up to 25 km to 30 km high. The radiosondes were released at the lidar field site in Naqu twice a day at 0000 and 1200 UTC.

Eleven weather balloons with Vaisala RS92 radiosondes (Vömel et al., 2007) have been launched to provide profiles of air temperature, relative humidity (RH), wind speed and wind direction usually up to the mid stratosphere. The RH can be measured between 0 and 100% with a resolution of 1% and an accuracy of 5% at -50 ℃ (Miloshevich et al., 2006; Wähn et al., 2004). While Miloshevich et al. (2009) found that the RH measured by RS92 has a moist bias in the lower stratosphere (LS) and a dry bias in the upper troposphere (UT). To quantify the accuracy of RH measurement by RS92 over the Tibetan Plateau, we compared RS92 RH measurements with simultaneous water vapor measurements from a Cryogenic Frostpoint Hygrometer (CFH) on 13 August 2011. The CFH is a lightweight (400 g) microprocessor-controlled instrument and operates on the chilled-mirror principle using a cryogenic liquid as cooling agent. It includes several improvements over the similar NOAA/CMD instrument. It is currently designed to be combined with ozone sondes to provide simultaneous profiles of water vapor and ozone (Vömel et al., 2007). CFH has been taken in many inter comparison experiment as an absolute reference for water vapor measurements, including the validation of Aura MLS water vapor products. After applying the time-lag and solar radiation bias corrections, corrected RS92 RH measurements show agreement with CFH in the troposphere. The mean difference between corrected RS92 RH measurements and CFH is a dry bias of 2.9% in the ground layer, while the mean differences in 5-10 km, 10-15 km and tropopause transition layer region are 1%, 0.6% and 1.4% moist bias, respectively. Therefore, the accuracy of corrected RS92 RH measurements is comparable to the accuracy of CFH in the UTLS (Yan, 2012).

2.3 Satellite Observations

The Cloud–Aerosol Lidar with Orthogonal Polarization (CALIOP) onboard CALIPSO (Winker et al.,2003), is used to characterize aerosol extinction profiles in the UTLS, which is a three-channel (532 nm parallel, 532 nm perpendicular, 1064 nm) elastic lidar receiving light at the same wavelength as the emitted laser frequency. CALIOP sends short and intense pulses (1064 and 532 nm) of linearly polarized laser light downward towards the Earth. The atmospheric backscatter profile is retrieved at 60 m vertical resolution from 8–20 km with a horizontal resolution of 1 km. The Level 2 aerosol extinctions at 532nm of CALIOP (version 3.0) (available at http://www-calipso.larc.nasa.gov/tools/data_avail/) were used to compare with the ground based MPL on the Plateau. CALIOP data are selected over a 300 km×300 km square with a MPL location in its center.

We used the water vapor profiles observations (version 3.3) from the Microwave Limb Sounder (MLS) on the NASA Aura satellite (Waters et al., 2006). Aura MLS measurements include water vapor, ozone and carbon monoxide that are useful tracers of tropospheric and stratospheric air; these data have been used to document enhanced levels of carbon monoxide in the upper troposphere over the Asian monsoon (Li et al., 2005a; Filipiak et al., 2005) and also over the North American summer monsoon (Li et al., 2005b).

3 Results

Fig.1a shows one case of aerosol enhancement observations in UTLS in the whole day of 7 Aug 2011. The case is the typical situation observed frequently over the Tibetan Plateau during the TOAR campaign. At nighttime (2100-0700 LST), aerosol enhancements were detected at relative constant altitudes from 17.0 km to 18.5 km (a.m.s.l.) due to the higher signal to noise ratios (SNR) of lidar compared with the daytime. A Vaisala RS92 radiosonde was launched at 0656 UTC on 8 August and reached the tropopause at 17 km about 1 hour later. Fig.1b presents the temperature and RH measured by this sounding along with lidar. These rather thick aerosol layers had optical depths around 0.01 and occurred in the temperature range between -70 and -80 ℃. The radiosonde data indicate that the air in the aerosol layers was relatively dry with RH of about 5% above an abrupt decrease of RH around the tropopause, which is very similar to the other cases measured this month with maximum RH of 10%.

Fig.2 shows the vertical profiles of aerosol Scattering Ratios (SR) measured at Naqu during 6–26 August 2011, along with the daily mean profiles of temperature. The measurements display relatively high aerosol extinction coefficients in the UTLS, which are 4-9 factors higher than those at altitudes below and close to (even higher than, such as on 6 and 12 August) molecular scattering coefficients at the same altitude. Compared with SR profiles of Nabro volcanic aerosols from MPLNET, EARLINET, NDACC and Hefei stations during June and July (Sawamura et al., 2013), the maximum SR of aerosol layers in UTLS over the Tibetan Plateau are similar to that over Universitat Politècnica de Catalunya, Barcelona, Spain (41.39 °N, 2.11 °E) as one of EARLINET stations but larger than the other observations. The highest aerosol extinction coefficients in the UTLS over the Tibetan Plateau generally located at 18-19 km altitudes, which are 1-2 km higher than the tropopause. Tropopause temperatures ranged from -70 ℃ to -80 ℃, and the height of the tropopause varied from 80 hPa to 100 hPa (from 17 km to 18 km), during the observational period. Moreover, such relatively high aerosol extinction coefficients could extend over broad layers, ranging approximately 3-4 km.

The CALIOP aerosol extinction coefficients over UTLS are available for 12, 13, 18 and 20 August. Fig.3 compares the average extinction coefficient profile of MPL with that of CALIOP and shows a good agreement between the two instruments in both aerosol layers altitude and the value of extinction coefficient. In particularly，the MPL profiles show less standard errors at each vertical resolution altitude possibly due to the good SNR of MPL observed at an high altitude of the lidar station and clear atmospheric environment over the Tibetan Plateau.

Fig.4 shows time series of total AOD and its daily averaged results, which varied from 0.075 to 0.142 with maximum of 0.214 at 11:27 LST on 25 Aug. The percentage of AOD of the enhanced aerosol layers in total AOD each day is also overlapped in this figure as the bar. The total AODs were derived from a Microtops II Sun photometer collocated by lidar. The percentage of AOD varied between 5% (25 Aug) and 40% (12 Aug) with about 15% for most of days, and it would possibly be even greater due to the available Sun photometer measurements were available only in daytime, when more aerosols entry the atmosphere from the ground induced by stronger emissions from human activities. While the daily averaged AODs of the enhanced aerosol layers in UTLS over the Tibetan Plateau varied from 0.007 to 0.030 with all samples averaged value of 0.016. Compared to the observations from lidar networks such as EARLINET, MPLNET and NDACC in June 2011, soon after eruption of Nabro volcano, such AOD levels of UTLS over the Tibetan Plateau are the same as the globally averaged ones with an order of 0.018±0.009 and a range of 0.003 to 0.04 at 532 nm (Sawamura et al., 2013). However, the percentages of the UTLS AOD in the total AOD over the Tibetan Plateau are slightly higher than those observations, with the latter varying from 2% to 23% at 532 nm. This might be on account of more clean atmospheric environment over the Tibetan Plateau.

According to the period of occurrence of aerosol layers in UTLS, the continuous lidar observation can be split into two stages: 6 to 12 (S1) and 22 to 26 (S2) August 2011 for the continuous maintenance stages of aerosol layer. Between the two stages, the existence of low clouds decayed the lidar signal to the extent that available aerosol layer could not be observed in UTLS. Additionally, cirrus in the upper troposphere would increase the retrieval error of extinction coefficient of above aerosol layer, and these cases were also removed from the dataset. Fig.5. shows the daily variation in plateau monsoon index (PMI) and the seven-day averaged PMI time series from 1 July to 31 August 2011, with an overlap of cirrus occurrence (He et al. 2013) and AOD in UTLS. PMI is an indicator of the daily mean intensity of the Tibetan Plateau monsoon. A larger PMI value indicates stronger monsoon in summer, which can be determined as follows (Tang et al. 1984):

$$PMI=H_1+H_2+H_3+H_4-4H_0 \quad (2)$$

where H is the daily deviation from the monthly mean geo-potential height at 600 hPa. The subscript numbers 0 to 4 indicate the location of the Center (90 °E, 32.5 °N), West (80 °E, 32.5 °N), South (90 °E, 25 °N), East (100 °E, 32.5 °N) and North (90 °E, 40 °N) of the Plateau, respectively.

Many researchers have adopted the PMI to analyze the Tibetan Plateau monsoon variation. It is concluded that the index can reasonably describe the main characteristics of the Tibetan Plateau monsoon (e.g., Bai et al. 2001; Bai et al. 2005; Xun et al. 2011). These two stages might be caused by the different circulation systems due to an apparent time interval of about 10 days with PMI undergoing a substantial oscillation. During the first stage (from 6 to 12 August 2011), when the AOD decreased from 6 to 7 August and increased from 8 to 12 August, the values of PMI experienced an increasing trend from -20 on 6 August to 63 on 12 August. The values sharply decreased to below -40 in the second stage with the low and continuous decreasing AOD over UTLS from 22 to 26 August 2011. Two obvious features can be found in the temporal variation of AOD: (i) AOD showed a decreasing trend companied by decreasing PMI during the campaign period, indicating that the aerosol layers wore off gradually with the reducing intensity of the Asian monsoon over the Tibetan Plateau at the end of August. Bourassa et al. (2012) found that the strong Asian monsoon anticyclone, which existed from June through September over Asia and the Middle East, where the Nabro volcanic aerosol was observed with OSIRIS, and the enhanced aerosol dispersed and quickly circulated throughout the Northern Hemisphere at the end of August, when the Asian monsoon anticyclone began to decay. And (ii) when the intensity of the Tibetan Plateau monsoon circulation subsided to PMI less than 0, the AOD in UTLS kept persistent decline regardless of the variation trend of PMI, indicating that confinement of the air in the lower stratosphere induced by Asian monsoon anticyclone were destroyed to benefit the enhanced aerosol dispersing to the whole Northern Hemisphere.

According to the previous studies, deep convective activities are also considered to play an important role for transporting aqueous solution droplets of troposphere into stratosphere. It has been verified that deep convection over the Tibetan Plateau is likely to be a primary pathway for water vapor from the maritime boundary layer (e.g., Indian Ocean, South China Sea). Dessler and Sherwood (2004) have also suggested that convective transport plays a key role for the accumulation of water vapor near the tropopause, resulting in an increase of H_2O mixing ratio by more than 5 ppmv near the tropopause (Gettelman et al., 2002; Park et al., 2004; Fu et al., 2006). But Tobo et al. (2007) used a growth model to calculate the possible growth under given atmospheric conditions assuming the existence of liquid solutions at equilibrium with respect to H_2O, H_2SO_4 and HNO_3, and found that aerosol growth is sensitive to H_2O mixing ratios. According to the calculated growth curves of liquid solutions as a function of temperature and water vapor, the high H_2O mixing ratios (more than 5 ppmv) are indispensable condition for producing high concentrations of fine particles near the tropopause. In fact, the H_2O mixing ratios near the tropopause from Vaisala RS92 radiosondes released in 6, 8 11 and 23 August 2011 are not more than 2 ppmv, obviously less than the previous observations, as shown in Fig.6. In consequence, the effects of gas-to-particle conversion from liquid solutions would likely be secondary to the enhancement of high tropopause aerosol extinction in these cases.

The continuous variation of water vapor distribution observed by satellite, despite lower vertical resolution, can also be used to investigate the contribution of liquid solutions conversion to the enhancement of high tropopause aerosol extinction. Fig.7 shows the time series of water vapor profile derived from MLS, tropopause level from sounder temperature profiles, and the altitude of daily mean maximum aerosol extinction coefficients in this region. It can be clearly seen that almost all the abundant water vapor transported by deep convective systems are concentrated below 120 hPa altitude (about 15 km). Meanwhile, the temporal correlation of extinction coefficients in aerosol layer with water vapor from day to day is weak with correlation coefficient of 0.36, suggesting that it is impossible that the enhanced tropopause aerosol is due to the condensation of water vapor.

In order to verify further that the enhanced tropopause aerosol is dominantly induced by the eruption of Nabro volcano, the aerosol loadings in UTLS over the Tibetan Plateau are compared with those over East China, where the influence of the Asian monsoon anticyclonic circulation and deep convection transportation were weak significantly. Table 1 listed some statistical parameters of aerosol layer over Tibet and Shanghai (31.23 °N, 121.53 °E) for the same period. The aerosol parameters over Shanghai were also derived from an MPL with the same mode used in the Tibetan Plateau. The larger averaged extinction coefficient and higher AOD of the aerosol layer in UTLS over Shanghai demonstrate that the enhanced tropopause aerosol was dominated by the Nabro volcanic emissions with quickly circulation throughout the Northern Hemisphere at the end of August when the Asian monsoon anticyclone began to decay.

4 Conclusion

In this study, we observed significantly increased aerosol extinction coefficients in UTLS over the Tibetan Plateau by continuous measurements with MPL during summer 2011. The retrieval of MPL showed a good agreement with CALIOP. The maximum SR of aerosol layers, up to 4-9, in the UTLS generally located in 18–19 km m.s.l., 1–2 km higher than the tropopause, with broad layer depth ranging approximately 3–4 km. Daily averaged AODs of the enhanced aerosol layers in UTLS over the Tibetan Plateau varied from 0.007 to 0.030, which are at the same levels as the previous observations. The percentages of AOD for the enhanced aerosol layers in the total AOD are slightly higher than those observations by Sawamura et al. (2013).

The eruption of Nabro volcano is considered as an important factor to explain the enhancement of tropopause aerosols observed in summer over the Tibetan Plateau. The aerosol layers wore off gradually with the reducing intensity of the Asian monsoon over the Tibetan Plateau at the end of August and confinement of the air in the lower stratosphere induced by Asian monsoon anticyclone were destroyed to benefit the enhanced aerosol dispersing to the whole Northern Hemisphere. Deficiency in water vapor in UTLS indicates that the effects of gas-to-particle conversion from liquid solutions induced by deep convective activities would likely be secondary to the enhancement of high tropopause aerosol extinction in these cases.

It is must be noted that our interpretations are based on a short time observation. It is difficult to conclude that either one of the two processes is dominant due to lack of observations for trace gases. If further observations with more frequent soundings of water vapor and trace gases can be performed to investigate a correlation of high aerosol extinction with ambient temperatures, water vapor, trace gases, liquid solutions and transport processes, the result will be helpful in validating origination and mechanism of the enhanced aerosol extinction in UTLS.

Acknowledgements. This study was supported by Special Funds for Meteorological Research in the Public Interest (Grant Numbers: GYHY201106023, GYHY201006047 and GYHY201406001), the National Natural Science Foundation of China (NSFC, Grant Numbers: 40705013, 40975012 and41175020), the Shanghai Science and Technology Committee Research Special Funds (Grant Number: 10JC1401600). We thank all TOAR team members and the staff from the Tibet Meteorological Service for assisting our experiment work.

References

Bai, H. Z., Xie, J. N., and Li, D. L.: The principal feature of Qinghai-Xizang Plateau monsoon variation in 40 years, Plateau Meteor., 20, 22–27, 2001.

Bai, H. Z., Ma, Z. F., and Dong, W. J.: Relationship between Qinghai-Xizang Plateau region monsoon features and abnormal climate in china, Plateau Meteor., 16, 484–491, 2005.

Bourassa, A., Robock, A., Randel, W., Deshler, T., Rieger, L., Lloyd, N., Llewellyn, E., and Degenstein, D.: Large Volcanic Aerosol Load in the Stratosphere Linked to Asian Monsoon Transport, Science, 337, doi:10.1126/science.1219371, 2012

Borrmann, S., Solomon, S., Avallone, L., Toohey, D., and Baumgardner, D.: On the occurrence of ClO in cirrus clouds and volcanic aerosol in the t ropopause region, Geophys. Res. Lett., 24(16), 2011- 2014, 1997.

Campbell, J. R., Hlavka, D. L., Welton, E. J., Flynn, C. J., Turner, D. D., Spinhirne, J. D., Scott, V. S., and Hwange, I. H.: Full-time, eye-safe cloud and aerosol lidar observation at Atmospheric Radiation Measurement program sites: Instruments and data processing, J. Atmos. Oceanic Technol., 19, 431 – 442, doi:10.1175/1520-0426(2002)019<0431:FTESCA>2.0.CO;2. , 2002.

Clarisse, L., Coheur, P. F., Theys, N., Hurtmans, D., and Clerbaux, C.: The 2011 Nabro eruption, a SO2 plume height analysis using IASI measurements, Atmos. Chem. Phys. Discuss., 13, 31161-31196, doi:10.5194/acpd-13-31161-2013, 2013.

Dessler, A. E. and Sherwood, S. C.: Effect of convection on the summertime extra tropical lower stratosphere, J. Geophys. Res., 109, D23301, doi:10.1029/2004JD005209, 2004.

Dethof, A., O'Neill, A., Slingo, J. M., and Smit, H. G. J.: A mechanism for moistening the lower stratosphere involving the Asian summer monsoon, Q. J. R. Meteorol. Soc., 125, 1079– 1106, 1999.

Fernald, F. G.: Analysis of atmospheric lidar observations: Some comments, Appl. Opt., 23(5), 652– 653, 1984.

Filipiak, M. J., Harwood, R. S., Jiang, J. H., Li, Q., Livesey, N. J., Manney, G. L., Read, W. G., Schwartz, M. J., Waters, J. W., and Wu, D. L.: Carbon monoxide measured by the EOS Microwave Limb Sounder on Aura: First results, Geophys. Res. Lett., 32, L14825, doi:10.1029/2005GL022765, 2005.

Fu, R., Hu, Y., Wright, J. S., Jiang, J. H., Dickinson, R. E., Chen, M., Filipiak, M., Read, W. G., Waters, J. W., and Wu, D.: Short circuit of water vapor and polluted air to the global stratosphere by convective transport over the Tibetan Plateau, Proc. Natl. Acad. Sci. USA, 103,5664–5669, 2006.

Gettelman, A., Salby, M. L., and Sassi, F.: Distribution and influence of convection in the tropical tropopause region, J. Geophys. Res., 107(D10), 4080, doi:10.1029/2001JD001048, 2002.

Hanson, D. R., Ravishankara, A. R., Solomon, S.: Heterogeneous react ions in sulfuric acid aerosols: A framework for model calculations, J. Geophys. Res., 99(D2), 3615- 3629, 1994.

He, Q., C., Li, J., Ma, H., Wang, G., Shi, Z., Liang, Q., Luan, F., Geng, and X., Zhou: The properties and formation of cirrus clouds over the Tibetan Plateau based on summertime lidar measurements. J. Atmos. Sci. doi:10.1175/JAS-D-12-0171.1, 70, 901-915, 2013.

Highwood, E. J. and Hoskins, B. J.: The tropical tropopause, Q. J. R. Meterol. Soc., 124, 1579– 1604 ,1998.

Hoskins, B. J. and Rodwell, M. J.: A model of the Asian summer monsoon. Part I: The global scale, J. Atmos. Sci., 52, 1329– 1340, 1995.

Jackson, D. R., Driscoll, S. J., Highwood, E. J., Harries, J. E., and Russell, J. M.: Troposphere to stratosphere transport at low latitudes as studied using HALOE observations of water vapour 1992–1997, Q. J. R. Meteorol. Soc., 124, 169– 192, 1998.

Keim, E. R., Fahey, D. W., Delnegro, L. A., Woodbridge, E. L., Gao, R. S., Wennberg, P. O., Cohen, R. C., Stimpfle, R. M., Kelly, K. K., Hintsa, E. J., Wilson, J. C., Jonsson, H. H., Dye, J. E., Baumgardner, D., Kaw, S. R., Salawitch, R. J., Proffitt, M. H., Loewenstein, M., Podolske, J. R., and Chan, K. R.: Observations of large reductions in the NO/NOy ratio near the mid-latitude tropopause and the role of heterogeneous chemistry, Geophys. Res. Lett., 23, 3223-3226, 1996.

Kim, Y. S., Shibata, T., Iwasaka, Y., Shj, G., Zhou, X., Tamuraa, K., and Ohashi, T.: Enhancement of Aerosols near The Cold Tropopause in Summer over Tibetan Plateau: Lidar and Balloon-borne measurements in1999 at Lhasa, Tibet, China, in: Lidar Remote Sensing for Industry and Environment Monitoring III, edited by: Singh U. N., Itabe, T., and Liu, Z., Proceedings of SPIE, Hangzhou, China , 4893, 496-503, 2003.

Li, Q., Jiang, J., Wu, D., Read, W., Livesey, N., Waters, J., Zhang, Y., Wang, B., Filipiak, M., Davis, C., Turquety, S., and Wu, S.: Convective outflow of South Asian pollution: A global CTM simulation compared with EOS MLS observations, Geophys. Res. Lett., 32, L14826, doi:10.1029/2005GL022762, 2005a

Li, Q., Jacob, D., Park, R., Wang, Y., Heald, C., Hudman, R., Yantosca, R., Martin, R., and Evans, M.: North American pollution outflow and the trapping of convectively lifted pollution by upper-level anticyclone, J. Geophys. Res., 110, D10301 doi:10.1029/2004JD005039, 2005b.

Li, W. L. and Yu, S. M.: The characteristics of aerosol spatial and temporal distribution, radiation forcing and climate effect by numerical simulation over the Tibetan Plateau, Sci. in China (Series D), 31(Supp.), 300-307, 2001.

Miloshevich, L. M., Vömel, H., Whiteman, D. N., Lesht, B. M., Schmidlin, F. J., and Russo, F.: Absolute accuracy of water vapor measurements from six operational radiosonde types launched during AWEX-G and implications for AIRS validation, J. Geophys. Res., 111, D09S10, doi: 10.1029/2005JD006083, 2006.

Miloshevich, L., Vömel, H., Whiteman, D. N., and Leblanc, T.: Accuracy assessment and correction of Vaisala RS92 radiosonde water vapor measurements, J. Geophys. Res., 114(D11), doi: 10.1029/2008JD011565, 2009.

Müller, D., Ansmann, A., Mattis, I., Tesche, M., Wandinger, U., Althausen, D., and Pisani, G.: Aerosol-type-dependent lidar ratios observed with Raman lidar, J. Geophys. Res., 112, D16202, doi:10.1029/2006JD008292, 2007.

NASA: U.S. Standard Atmosphere Supplements, U.S. Govt. Print. Off., Washington, D.C.,1976.

Park, M., Randel, W. J., Kinnison, D. E., Garcia, R. R., and Choi, W.: Seasonal variation of methane, water vapor, and nitrogen oxides near the tropopause: Satellite observations and model simulations, J. Geophys. Res., 109, D03302, doi:10.1029/2003JD003706, 2004.

Rosenlof, K. H., Tuck, A. F., Kelly, K. K., Russell III, J. M., and McCormick, M. P.: Hemispheric asymmetries in water vapor and inferences about transport in the lower stratosphere, J. Geophys. Res., 102, 13,213– 13,234, 1997.

Sawamura, P., Vernier, J. P., Barnes, J. E., Berkoff, T. A., Welton, E. J., Arboledas, L. A., Guzmán, F. N., Pappalardo, G., Mona, L., Madonna, F., Lange, D., Sicard, M., Beekmann, S. G., Payen, G., Wang, Z., Hu, S., Tripathi, S. N., Jabonero, C. C., and Hoff, R. M.: Stratospheric AOD after the 2011 eruption of Nabro volcano measured by lidars over the Northern Hemisphere, Environ. Res. Lett., 7(3), doi:10.1088/1748-9326/7/3/034013, 2013

Solomon, S.: Stratospheric ozone depletion: a review of concept and history, Rev. Geophys., 37, 275-316, 1999.

Solomon, S., Borrmann, S., Garcia, R. R., Portmann, R., Thomason, L., Poole, L. R., Winker, D., and McCormick, M. P.: Heterogeneous chlorine chemistry in the tropopause region, J. Geophys. Res., 102(D17), 21411- 21429, 1997.

Tang, M. C., Liang, J., Shao, M. J., and Shi, G.: Preliminary analysis on the yearly variation of Tibetan Plateau monsoon, Plateau Meteor., 3, 76–82, 1984.

Tobo, Y., Zhang, D., Iwasaka, Y., Shi, G., Kim, Y., Ohashi, T., Tamura, K., and Zhang, D.: Balloon-borne observations of high aerosol concentrations near the summertime tropopause over the Tibetan Plateau, Atmos. Res., 84, 233-241, 2007.

Tukiainen, S., Kujanpää, J., Bingen, C., Robert, C., Tétard, C., and Dekemper, E.: Nabro volcano aerosol in the stratosphere over Georgia, South Caucasus from ground based spectrometry of twilight sky brightness, Atmos. Meas. Tech., 6, 2563-2576,doi:10.5194/amt-6-2563-2013, 2013

Uchino, O., Sakai, T., Nagai, T., Nakamae, K., Morino, I., Arai, K., Okumura, H., Takubo, S., Kawasaki, T., Mano, Y., Matsunaga, T., and Yokota, T.: On recent(2008–2012) stratospheric aerosols observed by lidar over Japan, Atmos. Chem. Phys., 12, 11975-11984, doi:10.5194/acp-12-11975-2012, 2012.

Vömel, H. H., Selkirk, L., Miloshevich, J., Valverde-Canossa, J., Valdes, J., and Diaz, J.: Radiation Dry Bias of the Vaisala RS92 Humidity Sensor, J. Atmos. Ocean. Tech., 24, 953–963, 2007.

Währn, J., Oyj, V., Rekikoski, I., Jauhiainen, H., and Hirvensalo, J.: New Vaisala Radiosonde RS92: Testing and Results from the Field, Eighth Symposium on Integrated Observing and Assimilation Systems for Atmosphere, Oceans, and Land Surface, Seattle, USA, 13 January 2004, 2004.

Waters, J. W., Froidevaux, L., Harwood, R. S., Jarnot, R. F., Pickett, H. M., Read, W. G., Siegel, P. H., Cofield, R. E., Filipiak, M. J., Flower, D. A., Holden, J. R., Lau, G. K., Livesey, N. J., Manney, G. L., Pumphrey, H. C., Santee, M. L., Wu, D. L., Cuddy, D. T., Lay, R. R., Loo, M. S., Perun, V. S., Schwartz, M. J., Stek, P. C., Thurstans, R. P., Boyles, M. A., Chandra, K. M., Chavez, M. C., Chen, G. S., Chudasama, B. V., Dodge, R., Fuller, R. A., Girard, M. A., Jiang, J. H., Jiang, Y., Knosp, B. W., LaBelle, R. C., Lam, J. C., Lee, K. A., Miller, D., Oswald, J. E., Patel, N. C., Pukala, D. M., Quintero, O., Scaff, D. M., Van Snyder, W., Tope, M. C., Wagner, P. A., and Walch, M. J.: The Earth Observing System microwave limb sounder (EOS MLS) on the Aura satellite, IEEE T. Geosci. Remote, 44, 1075– 1092, 2006.

Winker, D. M., Pelon, J., and McCormick, M. P.: The CALIPSO mission: Space borne lidar for observation of aerosols and clouds, Proc. SPIE, 4893, 1–11, 2003.

Wu, P.M., Okada, K., Tanaka, T., Sasaki, T., Nagai, T., Fujimoto, T., and Uchino, O.: Balloon observation of stratospheric aerosols over Tsukuba, Japan Two years after the Pinatubo volcanic eruption, J. Meteor. Soc. Jpn., 72, 475–480, 1994.

Xun, X. Y., Hu, Z. Y., Cui, G. F., He, H. G., Sun, J., Hao, L., and Gu, L. L.: Change of monsoon in Qinghai-Xizang Plateau and its correlation with summer precipitation of Ordos Plateau, J. Arid Land Resour. Environ., 25 (4), 79–83, 2011.

Yan, X. L.: The observation and study on the upper troposphere and lower stratosphere water vapor and ozone over Tibetan Plateau and its adjoint regions, master's thesis, Beijing: Chinese Academy of Meteorological Sciences, 2012.

Yanai, M., Li, C., and Song, Z.: Seasonal heating of the Tibetan Plateau and its effects on the evolution of the Asian summer monsoon, J. Meteorol. Sci. Jpn., 70, 319– 351, 1992.

Table 1 Statistical parameters of aerosol layer over Tibet and Shanghai. Maximum extinction coefficient (ECmax), Averaged extinction coefficient (ECave), aerosol layer depth(ALD), aerosol layer height over sea level and aerosol optical depth (AOD) of the aerosol layer from 20:00 to 06:00 local standard time (LST). The numbers in parenthesis correspond to the standard deviations.

	$EC_{max}(km^{-1})$	$EC_{ave}(km^{-1})$	ALD(km)	ALH(km)	AOD
Tibet	0.007	0.002(0.002)	3.604(1.626)	18.492(0.248)	0.016(0.002)
Shanghai	0.010	0.006(0.003)	4.380(0.764)	16.860(0.839)	0.027(0.006)

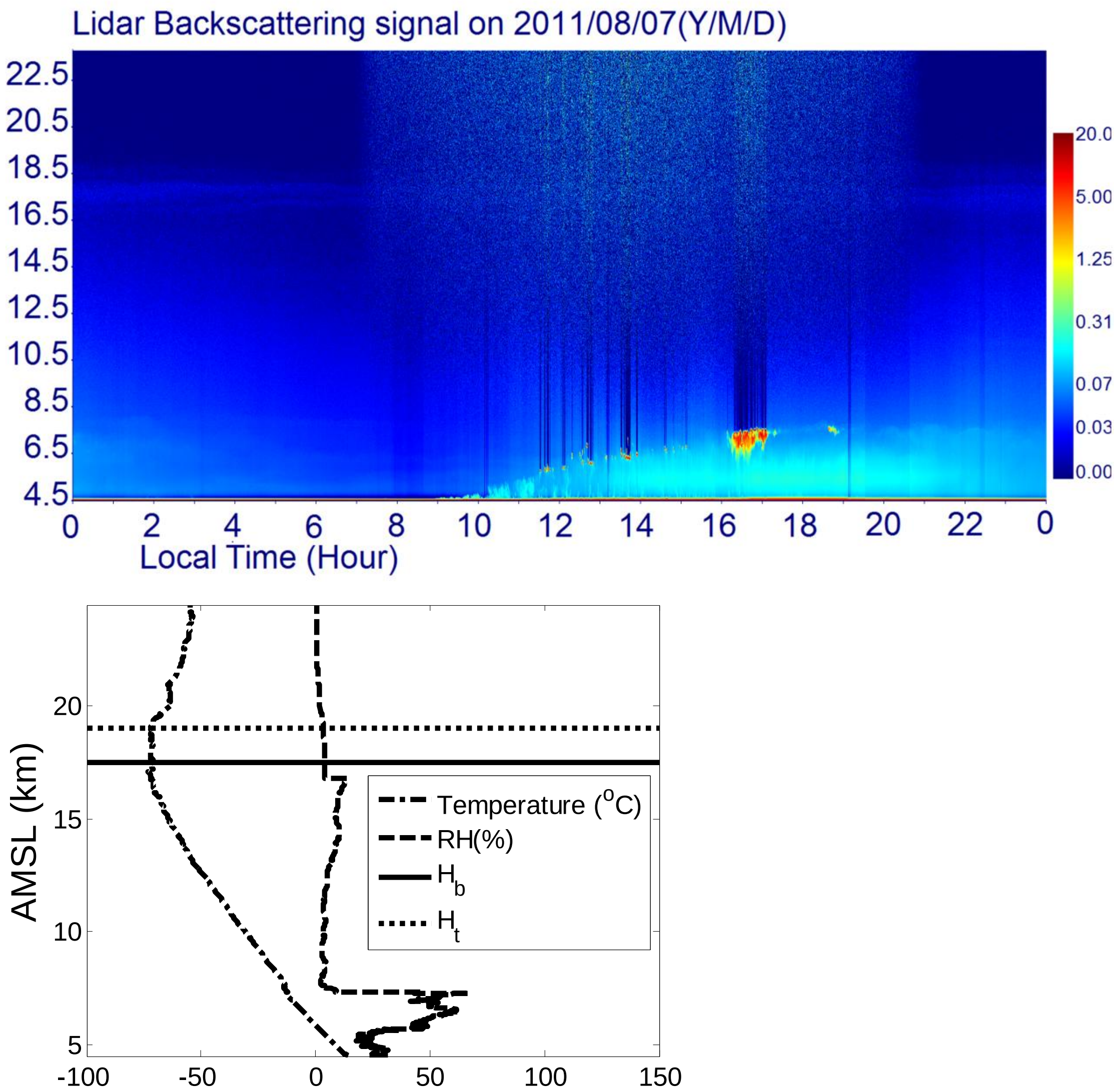

Fig.1. (a) One case of aerosol enhancement observations during the TOAR campaign. Range-corrected 532 nm signals are shown with 30 s and 30 m resolution. (b) Temperature and RH profiles measured by the RS92 radiosonde. H_t and H_b denote the mean top and base heights of aerosol layer, respectively.

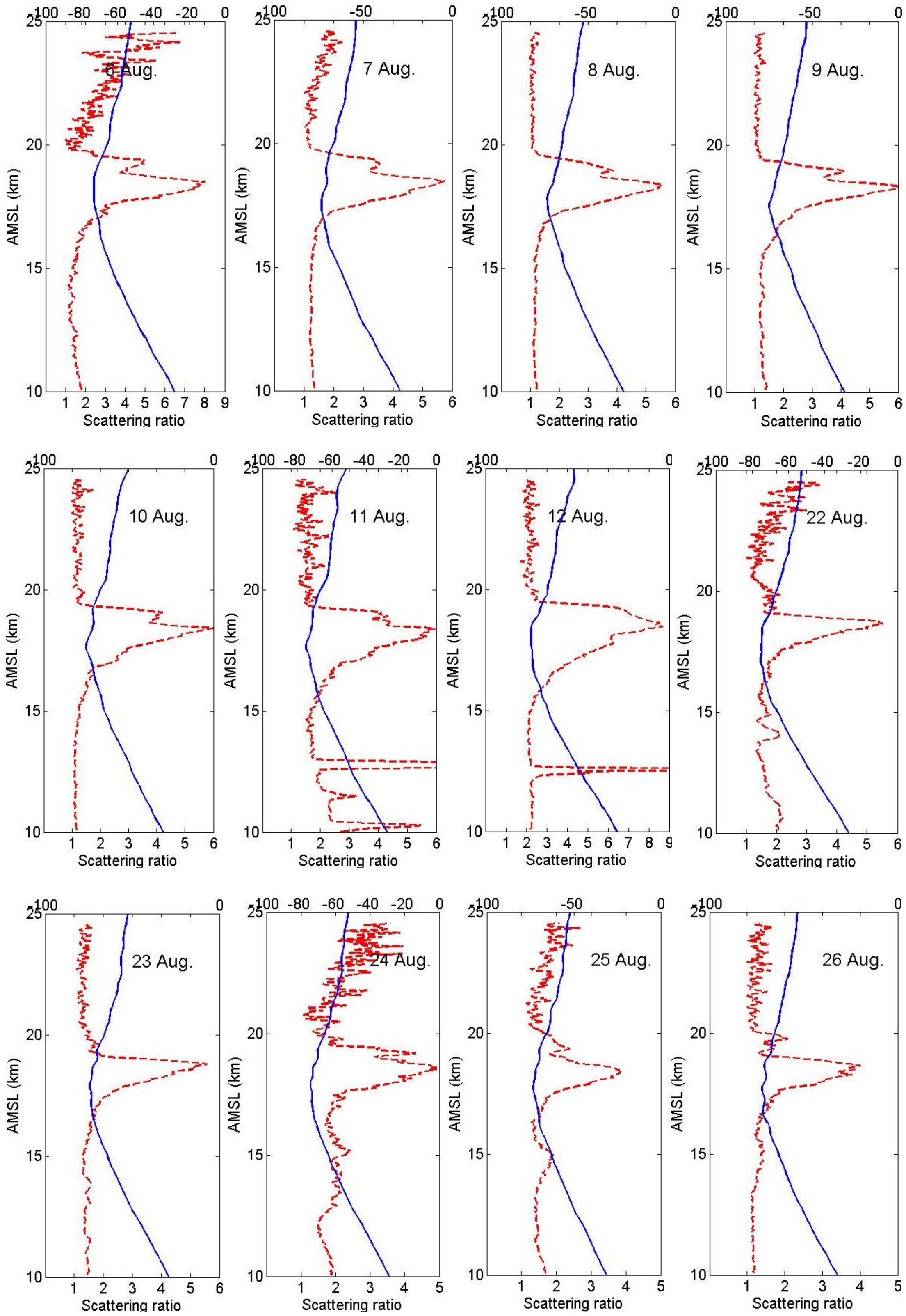

Fig. 2. The nighttime mean aerosol scattering ratio profiles (dashed line) from MPL. The daily mean profiles of temperature (solid line ℃) from the two radiosondes each day are overlaid to indicate the altitude of the tropopause (~18 km a.m.s.l.).

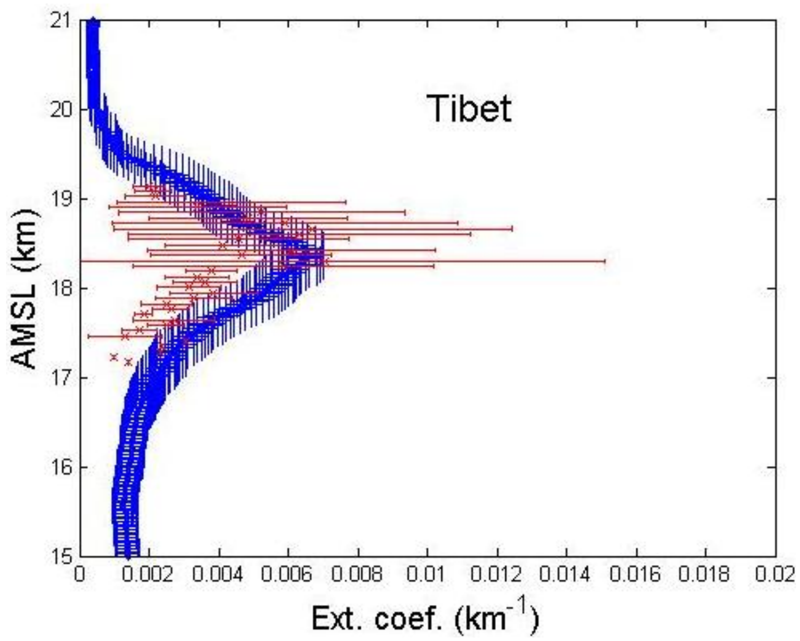

Fig.3. The average extinction coefficient profile of MPL (blue solid line) and the average extinction coefficient at each layer from CALIOP (red stars) during the whole observation period. The standard errors are marked as the error bar.

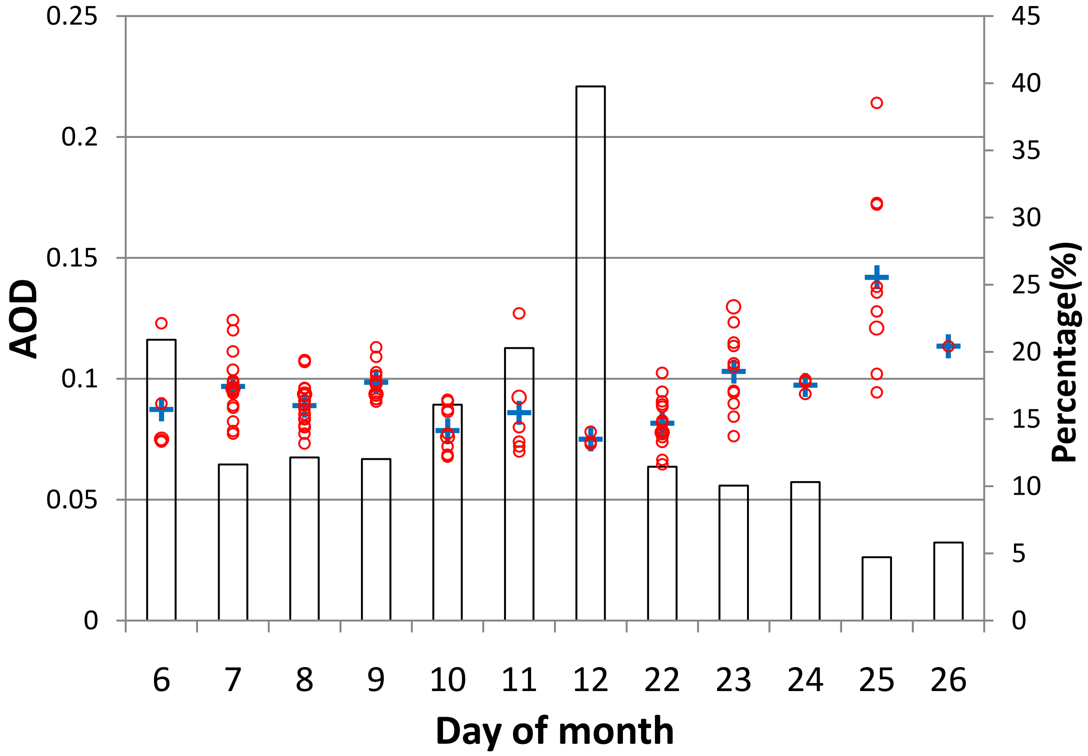

Fig.4. Time series of total AOD (o) and its daily averaged results (+) derived from Microtops II Sunphotometer. The percentage of daily averaged AOD of the enhanced aerosol layers in the total AOD is defined as the bar.

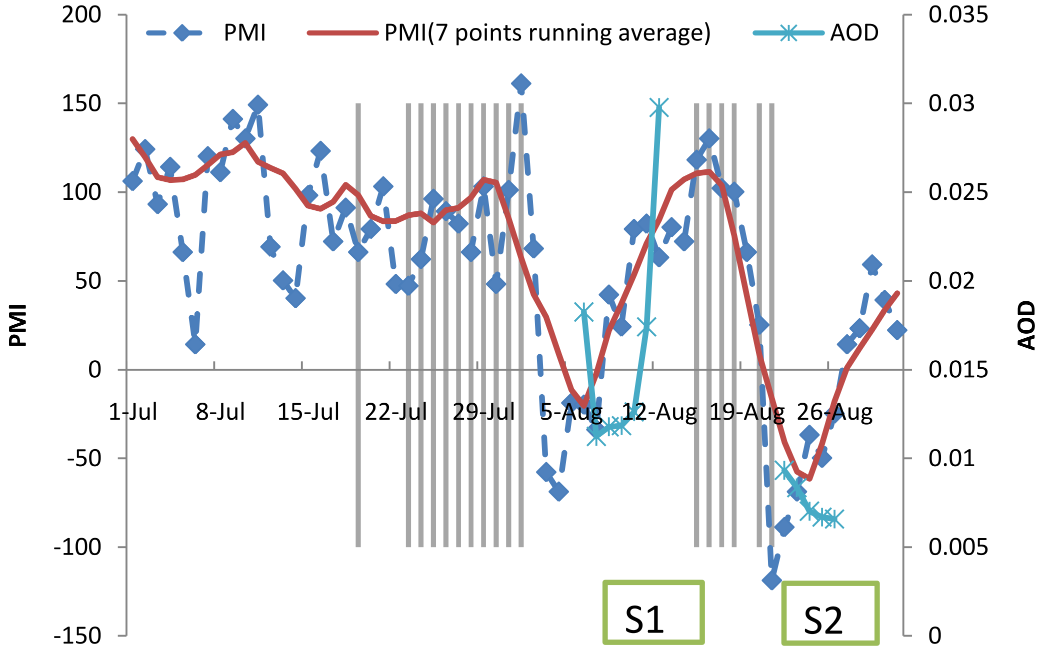

Fig.5. Daily variation of PMI and the 7-day-averaged PMI time series from 1 Jul to 31 Aug 2011and AOD in UTLS retrieved from MPL over the Tibetan Plateau. The days with cirrus occurrence are shaded (He et al. 2013). S1 and S2 represent two continuous maintenance stages of aerosol layer by lidar observation from 6 to 12 and from 22 to 26 August 2011, respectively.

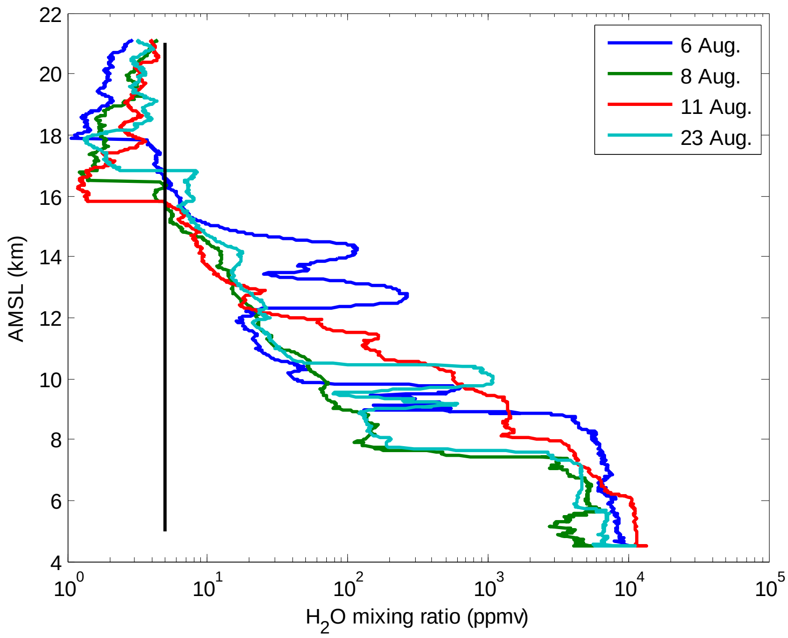

Fig. 6. Vertical profiles of water vapor from Vaisala RS92 radiosondes released in 6, 8, 11 and 23 August 2011, respectively. The black line along *y* axis represents the 5 ppmv of water vapor mixing ratio.

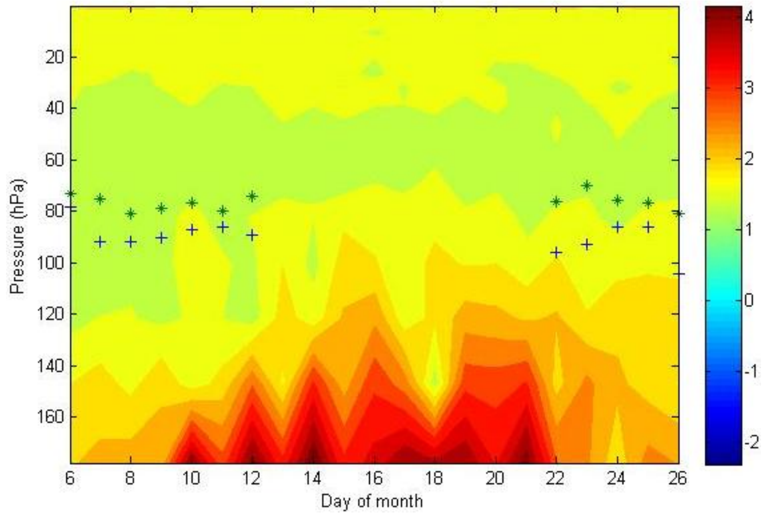

Fig. 7. Altitude-time distributions of MLS water vapor (ppmv, color bar in natural logarithm) from 6 to 26 August 2011. Stars indicate the layer with nighttime mean maximum extinction coefficient and pluses stand for the tropopause level of each day, respectively.